# AN AUTOMATED IMAGE PROCESSING ALGORITHM TO DETERMINE WRINKLE CHARACTERISTICS FROM B-SCANS

Anhadjeet Sandhu[1], Timothy J. Dodwell[1], Richard Butler[2]

[1]College of Engineering, Mathematics and Physical Sciences, University of Exeter, EX4 4SB, UK
Emails: as909@exeter.ac.uk, t.dodwell@exeter.ac.uk
[2]Department of Mechanical Engineering, University of Bath, BA2 7AY, UK
Email: r.butler@bath.ac.uk

**Keywords:** B-scan, wrinkle defect, large composite parts,

**Abstract**
This paper presents an automated algorithm which extracts wrinkle characteristics from B-Scan images of large composite parts. Out-of-plane ply misalignment is estimated by a bespoke fully automated algorithm based on the multiple field image analysis method (MFIA) . The original algorithm is adapted to (1) specifically improve the method's robustness at handling low resolution images typical of B-scan data and (2) compute wrinkle characteristics such as wavelength, amplitude and location. The algorithm is first validated against a synthetic wrinkle created using a localised wave function, and shows wavelength characteristics computed to within ±1%. The algorithm is then demonstrated for real scans of out-of-plane wrinkles in the corners of a large-scale C-section component. Finally, we show how the algorithm is used to generate a finite 3D representation of the wrinkles. It is envisaged this model can be used to assess component knockdown factors without the need for expensive destructive testing.

## 1. Introduction

Non-destructive testing and inspection of large scale composite structures is challenging. To assess defects, such as wrinkles [2] or porosity in manufactured parts, a popular option is B-scans; in which large scale parts with relatively simple geometries can be readily scanned in-situ. The extraction of defect data from scans is often a manual process which is time consuming and subject to observational bias.

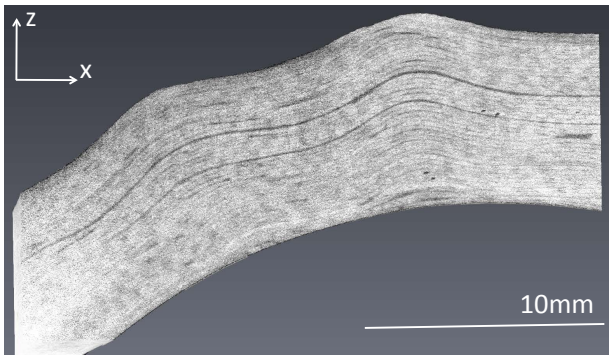


Figure 1: Example of wrinkles a curved geometry

Wrinkles appear during consolidation owing to the lack of interply slip as a result of physical constraints when forming curved parts, as seen in the CT scan in Fig.1 [3]. They may result in localised stress concentrations leading to failure at reduced loads. Since rejecting a defected component can be an expensive option, it becomes necessary to quantify a *knockdown factor* where it is important to obtain accurate and repeatable measurements for size and location of any defects if the data is to be used for certification or concessions purposes.

Fibre (mis-)alignment is estimated by a bespoke algorithm based on the multiple field image analysis

Excerpt from ISBN 978-3-00-053387-7

method (MFIA) proposed by Creighton *et. al.* [1, 4]. This method was selected over other possible choices (e.g. Hough Transformations [5] and classical fourier methods [6]) due its suitability in detecting fibre waviness [4, 7]. The workings of the algorithm are explained in section 2. Although fibre alignment is estimated using a method developed by Sutcliffe *et. al.* [4, 7], in section 2.2, it has been extended and adapted with the principle aim of improving the robustness at handling low resolution images typical of B-Scans (see Fig.8). Using an artificially created wrinkle and estimating its alignment field, section 2.3 demonstrates the techniques used to extract its wavelength, location and amplitude. Based on extracted results, one of the samples was reconstructed to yield the meshed FE model shown in section 3.

## 2. Methodology and demonstration of the algorithm

This section describes, in depth, the mapping between curved geometries and flat scans followed by the approximation of the alignment map. Based on the map, wrinkle characteristics are determined and used to reconstruct models and meshes to enable finite element calculations. The method is demonstrated using a synthetically generated wrinkle, see Fig.4 (lower) using the localised wave function,

$$g(x, y) = \mathbf{A}(y)\,\mathrm{sech}^2(\xi_1 x)\cos(\xi_2 x) \tag{1}$$

The grey scale function of a binary image simulating the perfect B-scan of layered media is defined as,

$$\mathcal{G}(x, y) := \begin{cases} 0 & \text{iff } \lceil \frac{\hat{y}}{t} \rceil \in \{1, 3, 5, \ldots, n\} \\ 1 & \text{iff } \lceil \frac{\hat{y}}{t} \rceil \in \{2, 4, 6, \ldots, n\} \end{cases} \tag{2}$$

where $t$ is the thickness of the scan, $\hat{y}$ is the ordinate such that $0 \leq \hat{y} \leq t$ and $n$ is the total number of layers and interfaces. A synthetic wrinkle may then be embedded using the transformation in (1).

### 2.1. Mapping from B-scan images to curved geometries

It is evident that scans taken on curved surfaces and flattened into 2D images must naturally condense data leading to distorted features. To recover the wrinkle characteristics, one must define the transformation from the rectangular coordinates of the B-Scan $(x, y)$ back to the part coordinates (e.g. $(s, n)$ arc length and normal to an arc as in Fig. 2). The algorithm presented is applicable to any geometric feature in which there exists a unique mapping between the two coordinate systems. This contribution considers a curved circular arc as shown in Fig. 2, for which the transformation is given by the mapping

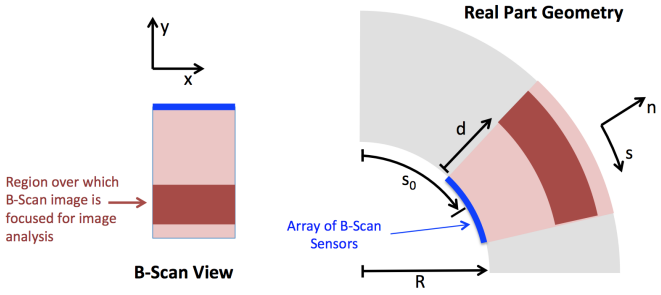


Figure 2: Transforming between a flat B-scan and a curved geometry

$$f : (x, y) \to (s, n) := \left(\left(1 + \frac{y}{R}\right)\left(s_0 + x - \frac{L}{2}\right), -y\right). \tag{3}$$

The Jacobian of $f$, defined as

$$\mathbf{J}_f(x, y) := \begin{bmatrix} 1 + y/R & R^{-1}\,(s_0 + x - L/2) \\ 0 & -1 \end{bmatrix} \tag{4}$$

gives the length scale changes as a result of the transformation $f$. The Jacobian is used to determine real wrinkle wavelengths and amplitudes, once extracted from the B-Scan image.

Excerpt from ISBN 978-3-00-053387-7

### 2.2. Estimation of fibre alignment using multiple field image analysis

The fibre alignment at a point $(x, y)$ is estimated by considering *trial fibres* of length $\ell$, centred about that point, orientated at $\theta$ to the horizontal. For each trial fibre orientation the average variation in grey-scale along the fibre, given by

$$\mathcal{J}(\theta) := \frac{1}{\ell} \int_{-\ell/2}^{\ell/2} |\mathcal{G}(0,0) - \mathcal{G}(\zeta,\theta)| \, d\zeta, \tag{5}$$

is calculated; where $\mathcal{G}(\zeta,\theta) \in [0,1]$ is the grey-scale at $(x + \zeta\cos\theta, y + \zeta\sin\theta)$ and $\zeta \in [-\ell/2, \ell/2]$ is the arclength parameter. The fibre alignment is the angle $\phi$ which minimises $\mathcal{J}(\theta)$ over all possible orientations $\theta \in [-90°, 90°]$. In practise the integral (5) is calculated using the trapezodial rule, whereby intermediate grey-scale values along the fibre length are interpolated from discrete pixel values. The minimisation is done using a (constrained) derivative free nonlinear optimiser as implemented in MATLAB's function `fmincon` [8].

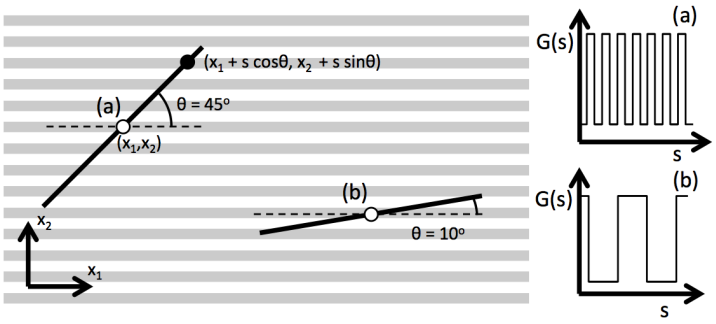


Figure 3: (left) Layered Example (Right) Plot of $\mathcal{J}$ against $\theta$

Figure 3 demonstrates how this algorithm works in practice. The left of the figure shows a simple layered material in which all layers are perfectly aligned with the $x$-axis. At point (a) a trial fibre orientation of $\theta = 45°$ is considered, the sub-plot shows how the grey scale varies rapidly over the fibre length, whilst at point (b) a trial fibre orientation of $\theta = 10°$ closer to the real orientation shows a much smaller variation in grey-scale. Figure 3 (right), shows a plot of $\mathcal{J}$ against $\theta$, which obtains a minimum at the true fibre orientation $\phi = 0°$.

The complete alignment field is approximated by calculating $\phi$ at $N$ randomly distributed points $(x^{(i)}, y^{(i)})$. A smooth approximation for $\phi(x, y)$ is generated by fitting a surface, defined on a uniform grid of size $h$ , to the data in the least square sense (see MATLAB's toolbox `gridfit` [9] ). These two steps are important enhancements to the algorithm that enable improved image processing of low resolution images typical of B-scan data. The initial evaluation of fibre alignments at randomly distributed points is important because it removes errors which arise as artifacts of the pixel grid. The smoothing (or surface fitting) process diminishes the influence of a single evaluation point, effectively damping highly localised misalignments on a scale smaller than the grid size $h$. Often such smaller scale features are non-physical and are simply a result of poor image resolution at that point. The resulting alignment map obtained from the test wrinkle is shown in Fig.4.

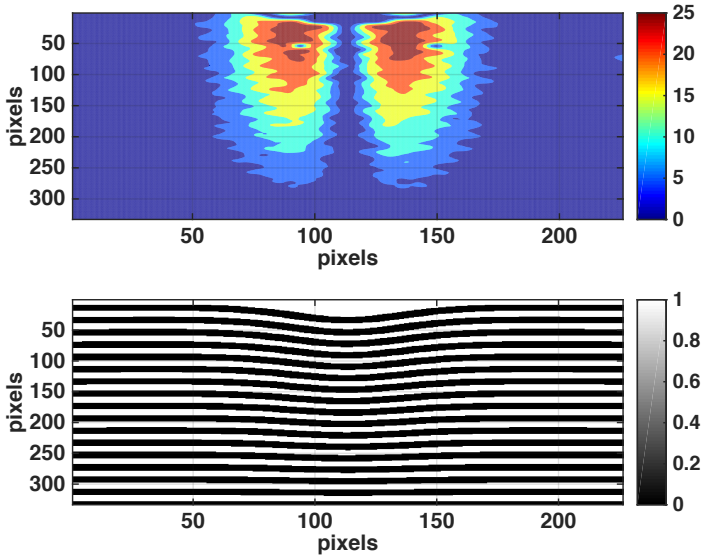


Figure 4: Above: Alignment map generated by the algorithm; Below: Synthetic wrinkle

Excerpt from ISBN 978-3-00-053387-7

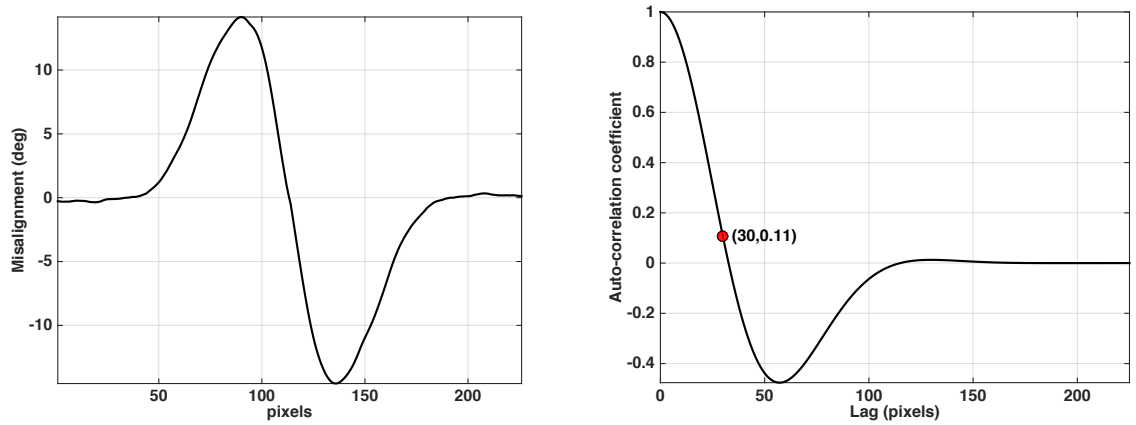


(a) Average wrinkle profile (b) Autocorrelation of the integrated signal

Figure 5: Estimation of wrinkle wavelength

### 2.3. Estimation of wrinkle wavelength, location and amplitude

To determine wrinkle characteristics it is useful to introduce the mathematical quantity $\Phi^n(x)$ such that,

$$\Phi^n(x) = \left(\frac{1}{L_2}\int_0^{L_2} \phi^n(x,y)\, dy\right)^{\frac{1}{n}} \tag{6}$$

where $\phi(x,y)$ is the alignment map and $L_2$ is its height. Obviously, $\Phi^1(x)$ is the average through thickness misalignment shown in Fig.5a. The wrinkle wavelength can then be estimated by calculating the auto-correlation function, see Fig.5b, of the misalignment map parallel to the layer direction

$$R(\tau) := \frac{\mathbb{E}[(\Phi^1(x) - \hat{\phi})(\Phi^1(x+\tau) - \hat{\phi})]}{\mathbb{E}[(\Phi^1(x) - \hat{\Phi}^1)^2]} \tag{7}$$

The wavelength is calculated as the lag-distance $\tau = \lambda$ at which the autocorrelation function is equal to $\alpha$ (i.e $R(\lambda) = \alpha$). From the literature on fibre waviness correlation lengths [7], surface roughness measures [10] and turbulent flow experiments [11] a value around $\alpha = 0.1$ is used. The suitability of this value can be seen in Fig.5.

Analytically, the *span* i.e. the $x$ expanse of the wrinkle or the central wave of the localised wave function $g(x,y)$ in the working example defined by (1) is

$$\lambda(g(x,0)) = 2.05mm \quad \text{for} \quad \mathbf{A}(0) = 0.25, \quad A(max) = 0, \quad \xi_1 = \xi_2 = 2 \tag{8}$$

whereas the algorithm approximates it to be $2mm$ resulting in an error of 2.5%. Here, the pixel dimensions in the x and y directions of Fig.4 (lower) are $\frac{6}{449}mm$ and $\frac{4}{338}mm$, respectively.

The average wrinkle, as defined by (6) for $n = 1$, reveals two distinct peaks that are useful in the quantification of its characteristics. The peaks represent the locations of maximum slope on either side of the wrinkle but the critical property of the waveform in Fig.5a is its period which is equal to the span of the wrinkle.

Before describing how the location of the wrinkle is found, two mathematical quantities are defined.

Excerpt from ISBN 978-3-00-053387-7

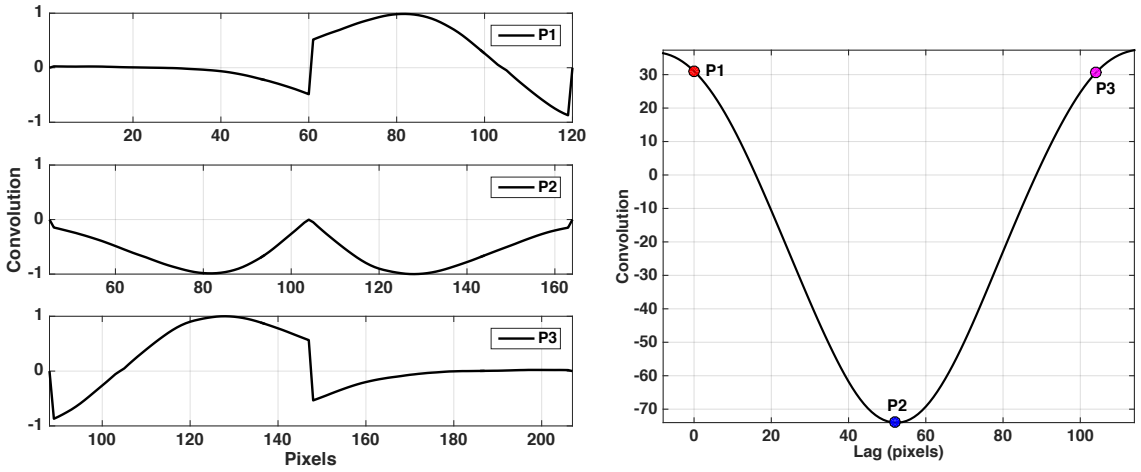


(a) Convolution between filter and signal

(b) Values of convolution function

Figure 6: Process of locating the wrinkle

Firstly, a stepped function $\chi_\Gamma$ for the set $\Gamma := [0, \lambda]$ where

$$\chi_\Gamma(x) := \begin{cases} 1 & 0 \leqslant x < \frac{\lambda}{2} \\ -1 & \frac{\lambda}{2} \leqslant x \leqslant \lambda \\ 0 & x \notin \Gamma \end{cases} \tag{9}$$

and secondly its cross-correlation with $\Phi^1(x)$ defined as

$$\left(\Phi^1 \star \chi_\Gamma\right)(\tau) := \int_{-\infty}^{\infty} \Phi^1(x)\chi_\Gamma(x-\tau)\, dx \tag{10}$$

for all lag values $\tau$. The location can be approximated by finding the value of $\tau \in [0, L_1]$, denoted $\tau^*$ which minimises the integral in (10) so that the centre of the wrinkle is at $x^* = \tau^* + \lambda/2$. $L_1$ is the length of the image in the x-direction in pixels. Figure 6 demonstrates how this process works.

*Remark: The cross-correlation* (10) *is defined as an integral over* $\mathbb{R}$*, yet the function* $\Phi$ *is defined over only a finite interval. In this case* $\Phi$ *is extended to the real line by zeros.*

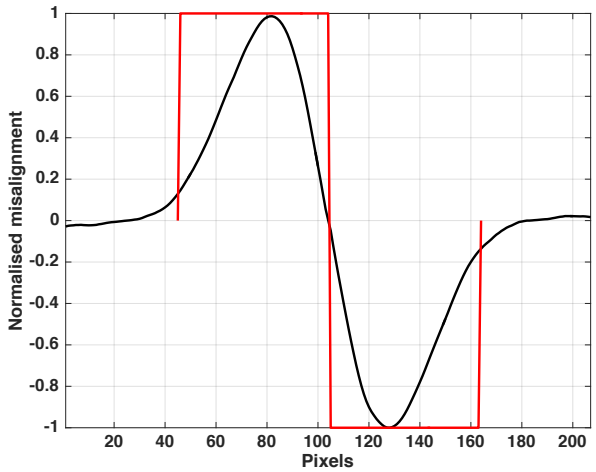


Figure 7: Filter position at P2

The convolution between $\chi_\Gamma$ and $\Phi$ has a distinct global minimum at P2, see Fig.6b. The corresponding position of the filter with respect to the intergrated signal (Fig.5a) is shown in Fig.7. P1 and P3 mark the extreme values of convolution for this particular signal. To locate the wrinkle, the filter is passed over the signal from left to right and then in reverse. The convolution function generated on both passes is averaged to yield Fig.6b. Moreover, asymmetric or non-prismatic wrinkles are better estimated by filtering the signal forwards and backwards. Additionally, the double step filter ensures that it only recognises a particular wrinkle and discards any feature that does not have the same span although there are some exceptional cases where the filter may fail.

Excerpt from ISBN 978-3-00-053387-7

Finally, the average wrinkle amplitude is approximated by the function below when $n = 1$,

$$A_n = \int_{x^*-\lambda/2}^{x^*} \tan \Phi^n(x)\, dx \tag{11}$$

With the defect located, the map of one half of the wrinkle is extracted for further processing. The average wrinkle amplitude described by (12) is $0.126mm$ which is within 1% of the analytical solution, $0.125mm$. In this example or other similar data, the mean is not a very useful estimate. The maximum amplitude can be estimated by evaluating (6) and (12) for $n > 1$ where the mean tends towards the maximum with increasing $n$. The function is convergent and $A_{200} = 0.241mm$. In comparison with the analytical solution, the error in the maximum amplitude is within ±5%.

## 3. Results

The B-scan shown in Fig.8 give an idea of the poor signal to noise ratio across the image with the exception of a thin band of relatively high quality in the upper half of the scans. The analysis was carried out only on this region of interest (ROI). By inspection one can say that the amplitude or span of the wrinkle within the ROI is not highly varied. Combined with the imaging error, the average wrinkle profile across the ROI is the most reliable set of data to use for the estimation of wavelength and location. Furthermore, anomalies like ply discontinuities or other highly localised features are less likely to have an influence on the result. Consequently, the measured average span of the wrinkle in Fig.8 is $3.6mm$ with an amplitude of $0.17mm$ over the ROI. However, it must be iterated that the algorithm only returns the largest of the wrinkles in cases where multiple defects are present.

The accuracy of the results depends on the number of sampling points amongst other parameters. Each run of the algorithm has an element of randomness to it which derives from the random selection of sampling points. The results presented in this paper were obtained using a distribution of points such that there was virtually no randomness.

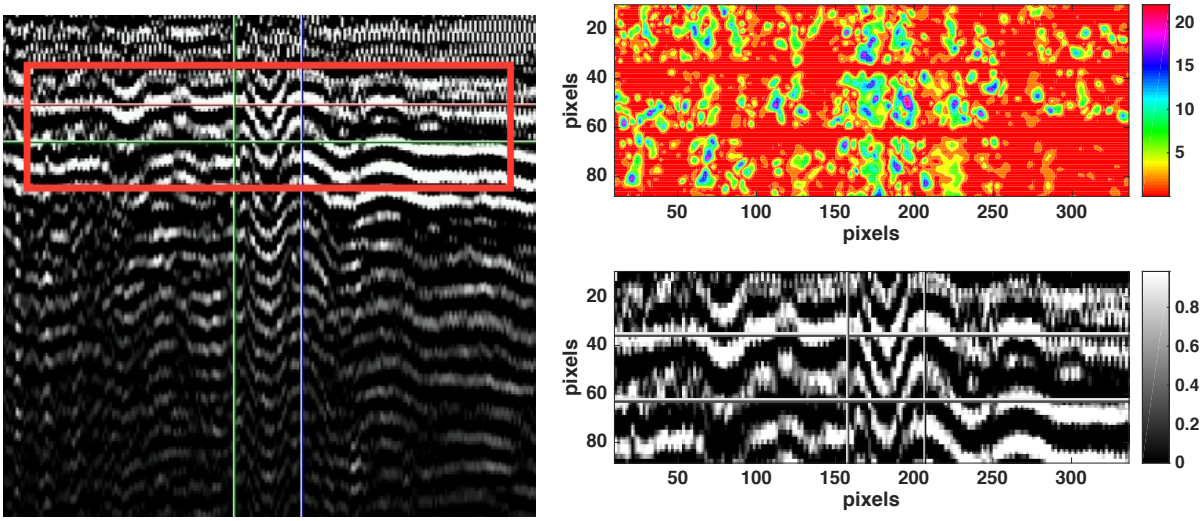


(a) Sample coupon lf024

(b) Alignment map of the highlighted section of 8a

Figure 8: Real B-scan

*Remark: The pixels in Fig.8 represent approximately 8 times the distance in the y-direction compared to the x-direction making the wrinkles appear much larger than they are.*

*A priori* knowledge of the scan geometry along with the computed location and size of the defect enable

Excerpt from ISBN 978-3-00-053387-7

a 2D reconstruction which is prismatically extruded into the third dimension. Using Gmsh the focussed region is reconstructed as opposed to the entire scan area. Modifying the limits of (12) to

$$A_n = \int_{x^*-\lambda/2}^{x_i} \tan \Phi^n(x)\, dx \quad \text{for} \quad x^* - \lambda/2 \leq x_i \leq x^* \tag{12}$$

where $x_i$ is any point within the span of the wrinkle, enables a series of points to be defined in the x-y plane and splines fitted to them creating ply boundaries. Each ply is defined as a separate surface bounded by its respective splines. Surfaces can be extruded to form volumes with unique labels. Any feature in the 2D geometry gets extruded prismatically. The reconstructed model can be padded with additional layers on both sides symmetrically or otherwise wherein the wrinkle is assumed to decay linearly to zero amplitude at the boundaries. 5 plies constitute the focussed region of Fig.9 padded with 3 plies on the inner arc and 7 on the outer side. FE analysis can be carried out on such a mesh as shown by the work of Fletcher *et. al.* [12]

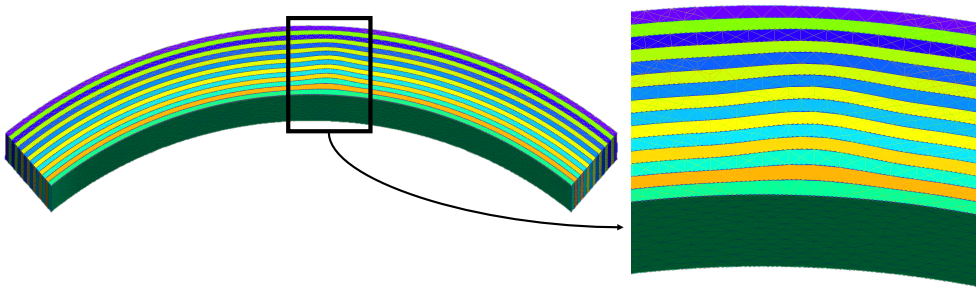

Figure 9: lf024 reconstructed

## 4. Concluding remarks

Wrinkles, amongst other defects, can often lower the strength of a composite part significantly. With the cost involved in destructive testing, an alternative solution is highly desirable. This paper presents a method of extracting wrinkle characteristics like wavelength and span from B-scans automatically providing the advantage of repeatability and reliability which are important if concessions are to be made on the part strength based on a wrinkle. The strength of the algorithm lies in its ability to handle low resolution data typical of B-scans. The wavelength, span and location of the test wrinkle show good agreement with the analytical results. The data obtained from B-scan also agrees well with the manually extracted data. With models reconstructed from actual scan data, such defects can be analysed using finite element methods much more accurately thus enabling manufacturers to make better predictions of *knockdown factors*.

## References

[1] P. Morgan. *Carbon fibers and their composites*. CRC Press Taylor & Francis Group, 2005.

[2] H. Koerber, J. Xavier, P.P. Camanho, Y.E. Essa, and F. Martín de la Escalera. High strain rate behaviour of 5-harness-satin weave fabric carbon-epoxy composite under compression and combined compression-shear loading. *International Journal of Solids and Structures*, 54:172–182, 2015.

[3] T.J. Dodwell, R. Butler, and G.W. Hunt. Out-of-plane ply wrinkling defects during consolidation over an external radius. *Composites Science and Technology*, 105:151 – 159, 2014.

Excerpt from ISBN 978-3-00-053387-7

[4] C. J. Creighton, M. P. F. Sutcliffe, and T. W. Clyne. A multiple field image analysis procedure for characterisation of fibre alignment in composites. *Composites:Part A*, 32:221–229, 2001.

[5] J. Illingworth and J. Kittler. A survey of the hough transform. *Comp Vision Graph Image Process*, 44:87–116, 1988.

[6] K. K. Kratmann, L. T. Lilleheden, R. Pyrz, and O. T. Thomsen. A novel image analysis procedure for measuring fibre misalignment in unidirectional fibre composites. *Compos Sci Technol*, 69:228–238, 2009.

[7] M. P. F. Sutcliffe, S. L. Lemanski, and A. E. Scott. Measurement of fibre waviness in industrial composite components. *Compos Sci Technol*, 72:2016–2023, 2012.

[8] J. C. Lagarias, J. A. Reeds, M. H. Wright, and P. E. Wright. Convergence properties of the nelder-mead simplex method in low dimensions. *SIAM J. Optim*, 9:112–147, 1998.

[9] John D'Errico. Surface fitting using gridfit. *MATLAB central file exchange*, 643, 2005.

[10] J. A. Williams. *Engineering Tribology*. Cambridge University Press, 2005.

[11] H. Tennekes and J. L. Lumley. *A first course in turbulence*. MIT Press, 1971.

[12] Timothy A. Fletcher, Tatiana Kim, Timothy J. Dodwell, Richard Butler, Robert Scheichl, and Richard Newley. Resin treatment of free edges to aid certification of through thickness laminate strength. *Composite Structures*, 146:26 – 33, 2016.

*Excerpt from ISBN 978-3-00-053387-7*